IRSTI 59.14.25 https://doi.org/10.26577/phst2024v11i2b05

Modeling and calibration of electrical features of p-n junctions based on Si and GaAs

J. Sh. Abdullayev[1]* and I. B. Sapaev[1,2]

[1]National Research University TIIAME, Tashkent, Kari Niyazov Street 39, 100000, Uzbekistan
[2]Western Caspian University, Scientific researcher, Baku, Azerbaijan
*e-mail: j.sh.abdullayev6@gmail.com
(Received August 7, 2024; received in revised form October 28, 2024; accepted November 22, 2024)

This study provides a detailed analysis of the temperature-dependent electrophysical properties and current-voltage (I-V) characteristics of p-n junction structures based on Silicon (Si) and Gallium Arsenide (GaAs). The investigation spans a temperature range of 0–1000 K, examining key parameters such as bandgap, mobility, intrinsic carrier concentration, and I-V characteristics. Advanced modeling and calibration techniques were employed to reveal intricate thermal dependencies of these parameters and their impact on device behavior. The results demonstrate that recombination currents dominate at low forward biases (0.1–0.3 V), characterized by an ideality factor near 2, while diffusion currents prevail between 0.3–0.7 V, with an ideality factor approaching 1. At higher voltages, high-injection conditions emerge. In Si, diffusion mechanisms dominate from 0.4–0.7 V, while in GaAs, recombination remains the primary mechanism up to 1.2 V. These findings are corroborated by semi-logarithmic I-V curves, illustrating the distinct transitions between current mechanisms. This comprehensive study highlights the robustness of the proposed models in accurately capturing the temperature-dependent behavior of these materials. The insights gained offer valuable implications for optimizing p-n junction-based devices across a wide temperature range. Future research will extend these models to explore more advanced semiconductor structures and operational scenarios.

Key words: p-n junction, Si, GaAs, calibration, cryogen temperature, bandgap, mobility, intrinsic concentration, I(V) curve, ideality factor.
PACS number(s): 73.40. Lq, 73.61.C w, 73.61. E y, 72.20. Jv

1 Introduction

Semiconductor devices, particularly p-n junctions, are integral components of modern electronic systems. Accurate modeling and calibration of the electrophysical properties of Si and GaAs are essential for optimizing device performance. Temperature is one of the most important parameters that externally affect the electrophysical properties of semiconductor materials. This article details the methodologies for modeling and calibration, offering insights into the unique characteristics exhibited by Si and GaAs p-n junctions. These methodologies enable a thorough exploration of temperature-dependent behaviors, enhancing our understanding of semiconductor physics and influencing the design of electronic systems. The use of these simulation tools allows for a more nuanced understanding of the complex interactions within semiconductor materials. Semiconductor materials are selected based on their wide application in semiconductor devices. The most crucial electrophysical parameters include the band gap, intrinsic carrier concentration, and the mobility of electrons and holes, along with current-voltage characteristics. In this paper, we focus on analyzing the features of semiconductor materials such as Si and GaAs. The mechanisms within the p-n junction are examined through the analysis of the I(V) characteristic and ideality factor. As is known, the band gap of semiconductor materials depends on several factors, such as temperature [1-3], geometric size [4, 5], and particle size in semiconductor nanomaterials [6]. The p-n junctions of Si and GaAs are well-studied, and the I(V) characteristics under forward bias are explained both experimentally and through modeling [7-12]. Investigating the ideality factor of p-n junctions is an established method for explaining current mechanisms [13-16]. However, many formulas for calculating the ideality factor in p-

n junctions are not well-explained across a wide range of both reverse and forward voltages. By studying existing models and developing new ones, we aim to address these shortcomings more effectively. Semiconductor devices can be modified in terms of geometry, materials, and structure. The subsequent sections of this article outline the methodologies employed for modeling and calibration, present the results of the temperature-dependent analysis, and discuss the implications for the broader field of semiconductor electronics. We also discuss the temperature dependence of band gap, mobility of electrons and holes, intrinsic conductivity, and the I(V) current and ideality factor m(V) as a function of forward voltage.

2. Methods and theoretical background

In this section, we conduct a comprehensive analysis of both the material characteristics and the methodologies employed. The study delves into the temperature dependence of electrophysical parameters, including band gap, intrinsic carrier concentration, electrical conductivity, and mobility. Our investigation specifically aims to clarify the current transport mechanisms in Si and GaAs-based p-n junctions, using a method that calculates the ideality factor by considering drift-diffusion and generation-recombination current mechanisms.

2.1 Bandgap and intrinsic concentration

As previously mentioned, the Band Gap emerges as the most crucial parameter in semiconductor materials. Therefore, the equation (1) enables the calculation of the varying temperature of the bandgap for *Si* and *GaAs*. The formula for calculating the temperature dependence of the bandgap in semiconductor materials is typically described by the Varshni equation. It's expressed as:

$$E_g(T) = E_g(T=0) - \frac{\alpha \cdot T^2}{T+\beta} \quad (1)$$

where $E_g(T)$ and $E_g(T=0)$ are band gap at T and 0 K respectively, α and β are material-specific constants. This equation shows how the bandgap energy varies with temperature. The parameters α and β are experimentally determined constants for a particular semiconductor material. The results of our new model and the corresponding equation are depicted in Figure 1. The intrinsic concentration serves as a fundamental electrophysical parameter of semiconductor materials. The intrinsic carrier concentration n_i in a semiconductor is given by the equation:

$$n_i(T) = \sqrt{N_C(T) \cdot N_V(T)} \cdot \exp\left(-\frac{E_g(T)}{2kT}\right) \quad (2)$$

where: $N_C(T)$ and $N_V(T)$ are the effective density of states in the conduction band and the effective density of states in the valence band. $E_g(T)$ is the energy band gap, k is the Boltzmann constant and T is the absolute temperature. The values of $N_C(T)$ and $N_V(T)$ depend on the material and are often expressed as functions of temperature.

2.2 Mobility and intrinsic electrical conductivity

The significance of carrier mobility in semiconductors is at a high level, especially when working with semiconductor devices. Carrier mobility refers to the ability of charge carriers (electrons or holes) to move through a semiconductor material in response to an electric field. The mobility $\mu_{n,p}$ is expressed in units of *cm²/V·s* and is given by the formula (3a) and (3b): Semiempirical formulas (3a) and (3b) do not match the experimental results at temperatures below 50K.

$$\mu_n = \mu_{n_0}\left(\frac{T}{300}\right)^{-0.57} + \frac{7.4\cdot 10^8 T^{-2.33}}{1+0.88\left[\dfrac{N_D}{1.26\cdot 10^{17}\cdot\left(\dfrac{T}{300}\right)^{2.4}}\right]\cdot\left(\dfrac{T}{300}\right)^{-0.146}} \quad (3a)$$

$$\mu_n = \mu_{p_0}\left(\frac{T}{300}\right)^{-0.57} + \frac{1.36\cdot 10^8 T^{-2.33}}{1+0.88\left[\frac{N_A}{1.26\cdot 10^{17}\cdot\left(\frac{T}{300}\right)^{2.4}}\right]\cdot\left(\frac{T}{300}\right)^{-0.146}} \quad (3b)$$

Where N_A and N_D are acceptor and donor concentrations respectively, incomplete ionization has been considered in several studies [17, 18], but in this work, we assume that all N_A and N_D acceptor and donor ions are fully ionized. T is the temperature, μ_{p0} and μ_{n0} are constant values for material *Si* and *GaAs*. Several factors affect carrier mobility such as temperature [19-21], Masetti [22]. However, in this study, we exclusively utilized model mobility dependent on temperature. Materials with high charge carrier mobility are crucial for faster and more efficient electronic devices. Si and GaAs are commonly used semiconductors with relatively high carrier mobility. Carrier mobility plays a vital role in the design and optimization of semiconductor devices, such as transistors, diodes, and integrated circuits. At high electric fields, carrier velocity may saturate due to scattering effects. Understanding carrier mobility is essential for designing semiconductor devices that operate efficiently and reliably. Different operating modes and factors affecting mobility are key to optimizing semiconductor technology for various applications. Ordinarily, multiple sources of scattering, such as impurities and lattice phonons, are present concurrently. A widely used approximation is "Matthiessen's Rule, " which was originally formulated by Augustus Matthiessen in [23]. This rule combines the effects of different scattering mechanisms and is expressed as (4): The graphical representation of the result from expressions (3a) and (3b) are depicted in Figure 4, illustrating intrinsic electrical conductivity as a function of temperature.

$$\frac{1}{\mu_{total}(T)} = \frac{1}{\mu_{lattice}(T)} + \frac{1}{\mu_{impurity}(T)} + \frac{1}{\mu_{defect}(T)}\cdots \quad (4)$$

Another electrophysical parameter influenced by temperature is intrinsic conductivity. intrinsic electrical conductivity in semiconductors is strongly temperature-dependent. At low temperatures, very few electrons have enough energy to jump from the valence band to the conduction band, leading to low conductivity. As temperature increases, more electrons gain sufficient thermal energy to overcome the band gap, moving into the conduction band, and creating electron-hole pairs. This increase in charge carriers (both electrons and holes) causes the intrinsic conductivity to rise exponentially with temperature. Although this mathematical model was analyzed over a wide temperature range, the effects of incomplete ionization at low temperatures were not considered. This approach was chosen to first examine the model without accounting for incomplete ionization as an initial step, with plans to incorporate incomplete ionization in subsequent studies. The relationship is typically modeled as (5): Thus, the intrinsic conductivity increases with temperature as more carriers are thermally excited across the band gap. For the materials we have chosen, expression (5) corresponds to the equation for electrical conductivity as a function of temperature:

$$\sigma(T) = \sigma_0(T)\cdot\exp(-\frac{E_g(T)}{2kT}) \quad (5)$$

$\sigma(T)$ is the conductivity, $\sigma_0(T)$ is determined by expression (6), which indicates a linear dependence on temperature, and we have also considered that this expression is temperature-dependent. This expression (5) was analyzed in two cases: Case A, where $\sigma_0(T)$ is assumed to have a strong linear dependence on temperature, and Case B, where $\sigma_0(T)$ is considered temperature-independent. The difference between Cases A and B is presented and analyzed in Figure 3.

$$\sigma_0(T) = q \cdot (n(T) \cdot \mu_n(T) + p(T) \cdot \mu_p(T)) \quad (6)$$

Here, $n(T)$ and $p(T)$ are the electron and holes concentration, $\mu_n(T)$ and $\mu_p(T)$ are the electrons and hole mobility which represents the temperature dependence. If we consider equal intrinsic electrons and holes concentration $n_i(T) = p_i(T)$, expression (5) can be substituted with expression (7).

$$\sigma_i(T) = \sigma_{0i}(T) \cdot \exp(-\frac{E_g(T)}{2kT}) \quad (7)$$

The graphical representation of the result from expression (7) is depicted in Figure 3, illustrating intrinsic electrical conductivity as a function of temperature. The obtained results were derived by considering the temperature dependence of the electrophysical parameters in our model.

2.3 I(V) curve and ideality factor

The forward voltage curve can be divided into three distinct regions. At low voltage, the recombination mechanism predominantly influences the behavior. In the middle voltage range, the diffusion current mechanism takes precedence, while at high voltage, the high injection mechanism becomes dominant. The Shockley diode equation describes the current-voltage characteristic of an ideal p-n junction diode. The equation is given by:

$$J(T) = J_0(T) \cdot (\exp(\frac{qV_{p-n}}{mkT}) - 1) \quad (8)$$

Where J(T) is the diode current, J_0(T) is the reverse-bias saturation current. V_{p-n} is the applied voltage across the p-n junction, m is the ideality factor and unitless quantity, which is typically between 1 and 2, q is the charge of an electron. This equation provides a mathematical representation of the current-voltage relationship in a semiconductor diode under different bias conditions. The ideality factor of *p-n* and *p-i-n* junctions is determined by equation (9), but this expression is reliable and accurate only at voltages higher than 0.1 V.

$$m = \frac{q}{kT} \cdot \frac{dV}{d\ln(I)} \quad (9)$$

The barrier height $\varphi_k(T)$ of a p-n junction, also known as the built-in potential or contact potential, can be determined using the following formula:

$$\varphi_k(T) = \frac{kT}{q} \ln(\frac{N_A \cdot N_D}{n_i^2(T)}) \quad (10)$$

Where N_A and N_D are the acceptor and donor concentrations, respectively, $n_i(T)$ is the intrinsic carrier concentration. This equation characterizes the equilibrium state of a *p-n* junction, wherein no external bias is applied. The barrier height is contingent upon doping concentrations and temperature.

3. Simulation results and discussion

This section presents graphical representations of the formulas and results analyzed above, derived from our new model, accompanied by a thorough analysis and comparisons. Figure 1 illustrates the results obtained from our model, which accurately represents the temperature-dependent bandgap width of Si and GaAs. Modeling the variation of the bandgap width with temperature over a wide range is crucial for understanding material behavior. Similar to Si, the bandgap of GaAs decreases with temperature; however, GaAs retains its direct bandgap nature, while Si exhibits an indirect bandgap. The temperature-dependent bandgap significantly impacts carrier generation, intrinsic carrier concentration, and overall device performance, including applications in solar cells, diodes, and transistors. Silicon is widely preferred for most electronic applications due to its abundance and indirect bandgap, while GaAs is commonly employed in optoelectronic devices such as LEDs and lasers, thanks to its direct bandgap.

In the next steps, the expressions for intrinsic concentration (2). As a result, this becomes very important in our new model, which can explain these properties as functions of temperature. Figure 2 presents results from our new model and outcomes derived from expression (2), accurately depicting the temperature-dependent intrinsic concentration with of *Si* and *GaAs*. The intrinsic concentration at 300 K for *Si* and *GaAs* signifies the equilibrium concentration of charge carriers (electrons and holes) in these materials.

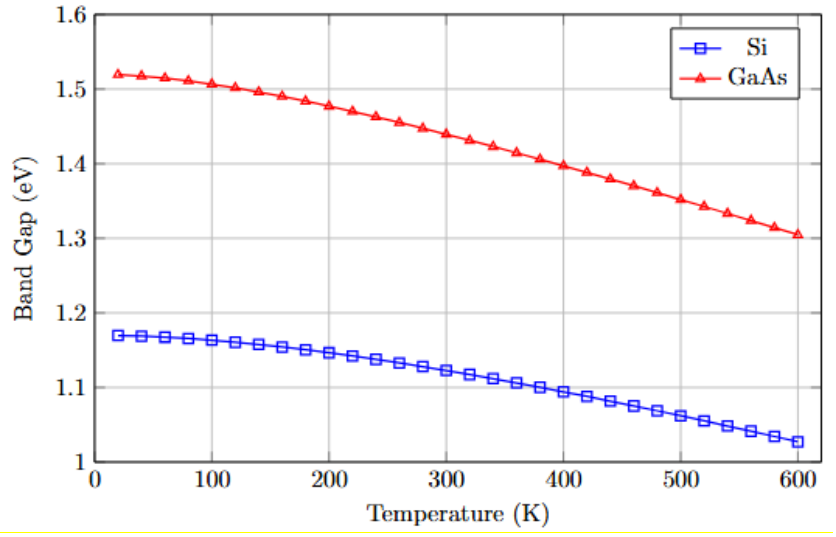

Figure 1 – Bandgap of a semiconductor as a function of temperature

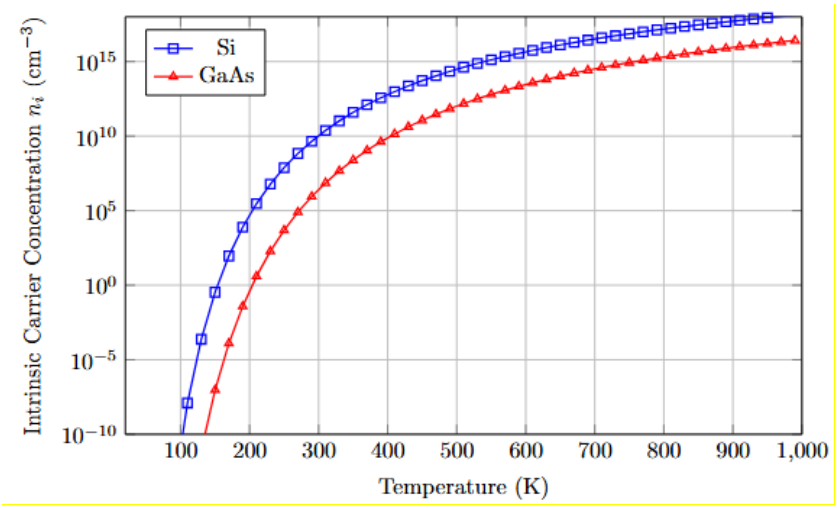

Figure 2 – The intrinsic carrier concentration of a semiconductor as a function of temperature

This intrinsic concentration, a characteristic property of semiconductors, is influenced by factors like the energy bandgap, temperature, and material-specific parameters. Understanding, intrinsic concentration is critical to analyzing the electrical behavior of semiconductors, particularly in devices like diodes and transistors. At low temperatures, not all dopant atoms are ionized, leading to incomplete ionization. Conversely, at high temperatures, full ionization occurs as all dopant atoms are ionized. Figure 2 shows at 300 K, $n_i = 1.5 \cdot 10^{10} [\frac{1}{cm^3}]$ for Si and $n_i = 2 \cdot 10^{6} [\frac{1}{cm^3}]$ for GaAs indicate the intrinsic carrier concentration.

By knowing the intrinsic concentration from expression (2), the intrinsic electrical conductivity can be determined using expression (7), which is shown as a function of temperature in Figure 3. The difference between state A and state B (6) lies in the value of the intrinsic conductivity, which reflects the strong temperature dependence of the expression. In state A, it takes a greater value compared to state B.

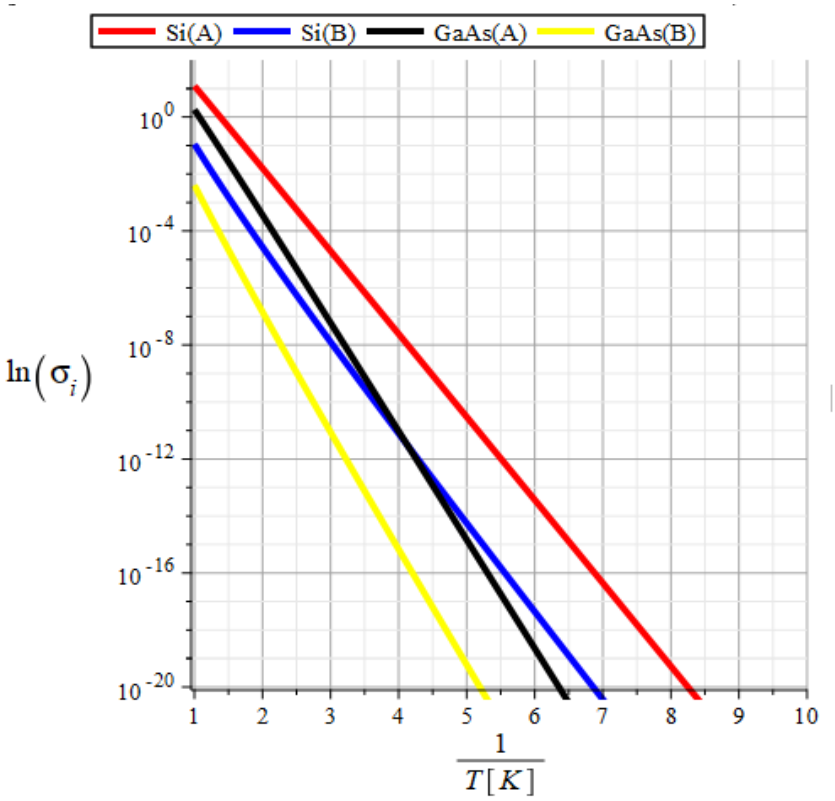

Figure 3 – Intrinsic conductivity of *Si* and *GaAs* as a function of temperature: In case (A) a strong temperature dependence was considered, while in case (B) a weak temperature dependence was taken into account

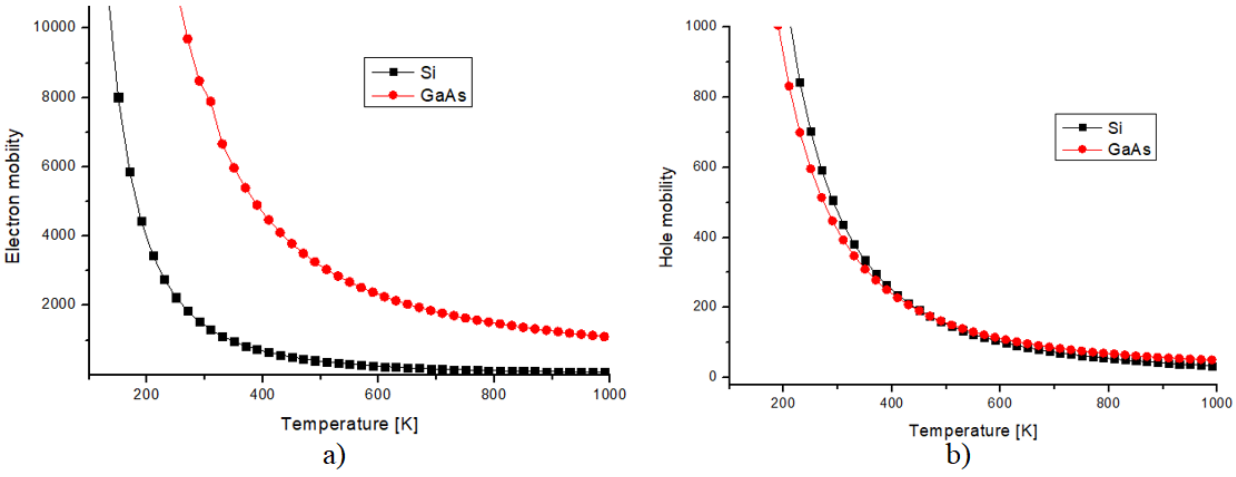

Figure 4 – The temperature dependence of carrier mobility for a) electrons and b) holes

Figure 4 illustrates a clear agreement between the mobility values derived from our new model and those obtained from reputable literature. Specifically, the electrons and holes mobilities $\mu_n = 1500[\frac{cm^2}{V \cdot s}]$ and $\mu_p = 450[\frac{cm^2}{V \cdot s}]$ for silicon (Si) and the electrons and holes mobilities $\mu_n = 8500[\frac{cm^2}{V \cdot s}]$ and $\mu_p = 400[\frac{cm^2}{V \cdot s}]$ for (GaAs) align closely with their respective literature values [24]. This indicates the reliability and accuracy of our new model in characterizing the mobility of electrons and holes in these materials.

Figures 5 and 6 showcase the I(V) characterristics of *Si* and *GaAs* materials, as determined by our new model. The drift-diffusion and generation-recombination models were incorporated into the simulation as current transport mechanisms. The temperature dependence of the band gap was calculated using the *Old Slotboom* mechanizm [25] and calibrated against experimental results for the selected Si material, as shown in Figure 5(a) [26]. By including the material parameters for GaAs, the new model produced the graph shown in Figure 5(b).

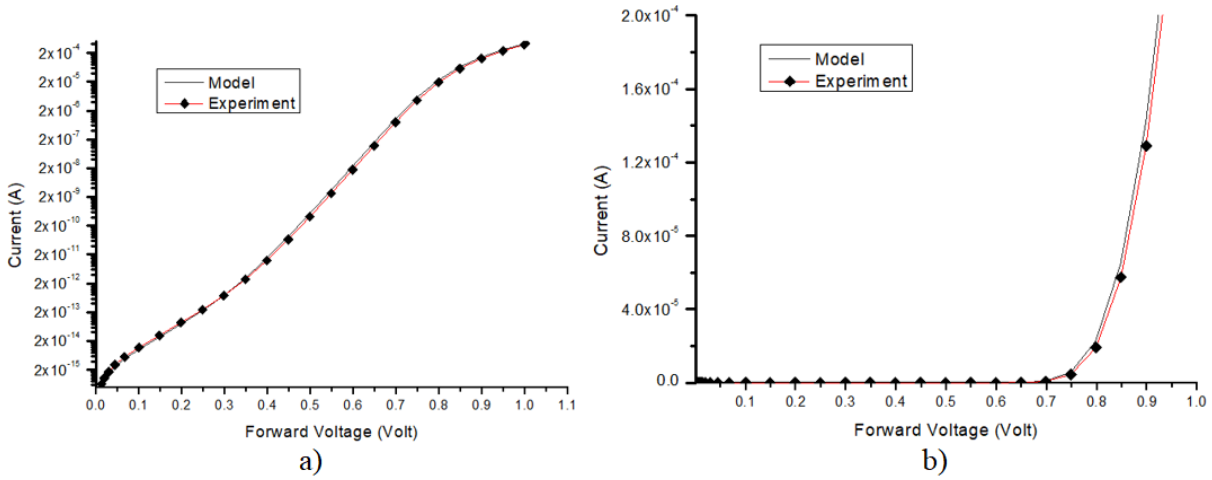

Figure 5 – a) Semilogarithmic I-V characteristics for the p-n junction based on Si, b) linear I-V characteristics for the p-n junction based on Si

Figure 5 illustrates that at low voltages, recombination current dominates up to 0.3 V, followed by diffusion current dominating up to 0.8 V. Beyond 0.8 V, the scenario shifts to high injection. Current (A) and voltage (V) characteristics are crucial for determining the current transfer mechanism and electrophysical processes in p-n junction structures. In the semi-logarithmic graph, the curvature of the curve between 0.1 and 0.3 V, and between 0.3 and 0.7 V at low voltage in forward bias, is explained by the current transfer mechanism. In this case, the ideality factor between 0.1 and 0.3 V takes a value close to 2, indicating a recombination mechanism. The ideality factor from 0.3 to 0.7 V is close to 1, signifying a diffusion mechanism.

Figure 6 depicts the *I(V)* characteristic of *GaAs* material, highlighting the series resistance effect above 1.3 V. Figure 5 and 6 a) the dominant region of the semi-logarithmic graph is commonly used to explain the current transport mechanism at low voltages. In the model, temperature dependence is considered for the strong A and weak B states. The voltage dependence of the ideality factor for both cases A and B is presented in Figure 7. It's important to note that this equation assumes ideal conditions and does not consider factors such as surface states or non-idealities present in real-world devices. In this paper, we calculated for Si $\varphi_k(T) = 0.823$ volt, for GaAs $\varphi_k(T) = 1.34$ volt by our model.

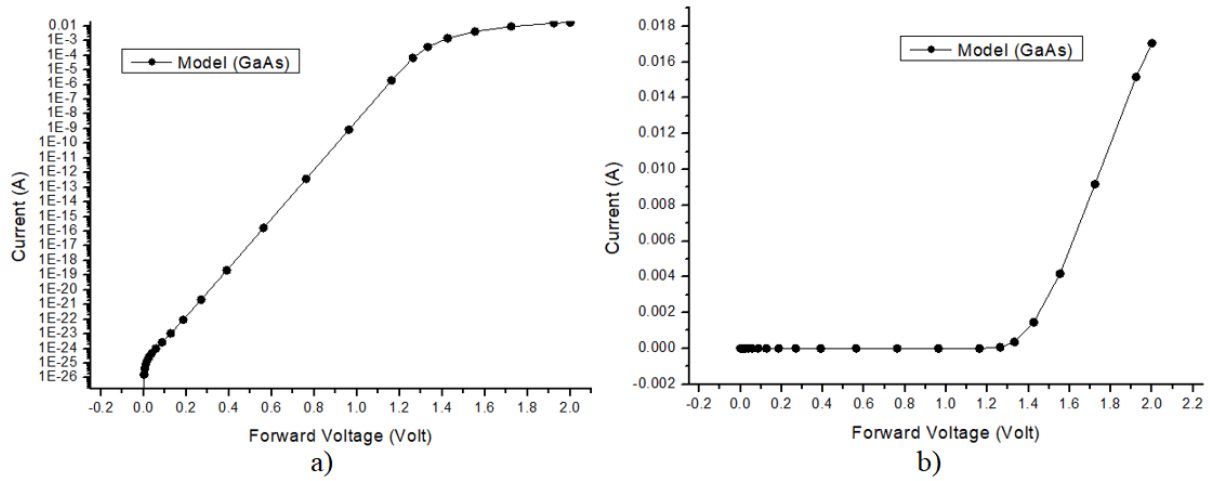

Figure 6 – a) Semilogarithmic I-V characteristics for the p-n junction based on *GaAs*, b) linear I-V characteristics for the p-n junction based on *GaAs*

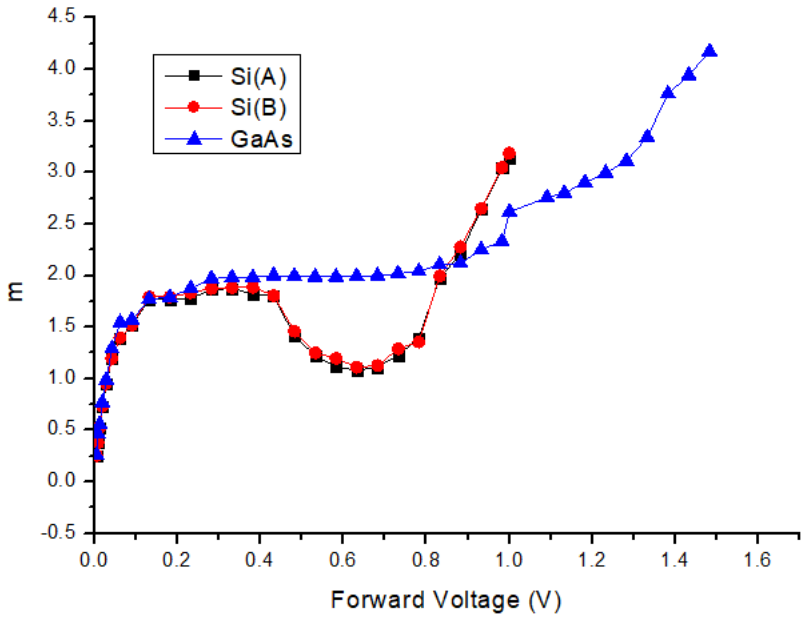

Figure 7 – Forward bias voltage dependent ideality factor for the p-n junction based on *Si(A), Si(B)* and *GaAs*

The ideality factor m is a dimensionless parameter that represents the deviation of the diode from ideal behavior. In an ideal diode, m would be equal to 1. However, in real-world diodes, m is often greater than 1, indicating non-ideal behavior such as recombination currents, series resistance, and other imperfections. Typically, m values range from around 1 to 2 for most diodes, but it can vary depending on the type of diode and its characteristics. Understanding and accurately determining the ideality factor is important in the analysis and modeling of diode circuits. Figure 7 displays the experimental results for *Si(A)* alongside the model results for *Si(B)* and our new model, as well as the results from the *GaAs* model. Analyzing the results for silicon (Si), it can be inferred that recombination mechanisms were predominant up to 0.4 V, while diffusion mechanisms prevailed up to 0.8 V. Due to GaAs's large band gap of 1.43 eV, the recombination mechanism was the dominant current mechanism from 0 V to 1.5 V.

3. Conclusion

In conclusion, our comprehensive investigation into the temperature-dependent properties of silicon (Si) and gallium arsenide (GaAs), achieved through meticulous modeling, calibration, and theoretical analysis, has yielded highly accurate findings. In the semi-logarithmic graph, the curvature of the curve between 0.1 and 0.3 V, and between 0.3 and 0.7 V, at low voltage in forward bias, is explained by the current transfer mechanism. In this context, the ideality factor between 0.1 and 0.3 V approaches 2, indicating a recombination mechanism. Conversely, the ideality factor from 0.3 to 0.7 V is close to 1, signifying a diffusion mechanism. We found that the temperature dependence of the internal electrical conductivity is stronger in case A than in case B. Furthermore, it was shown that in Si, the recombination mechanism dominates at low voltages between 0.1 and 0.3 V, while the diffusion mechanism prevails at higher voltages between 0.4 and 0.7 V. In GaAs, the recombination mechanism is dominant across the voltage range of 0.1 to 1.2 V. The robustness of our model is evident in its ability to accurately capture and predict the intricate behavior of these materials across a broad temperature range. Consequently, we envision utilizing this model in our future research endeavors.

References

1. Rahmouni S., Boubekri, H., Bendjeffal, H. et al. The temperature effect on the photoluminescence of porous silicon films obtained from an n-type silicon substrate // Silicon. – 2024. – Vol.16. – P. 4253–4261 https://doi.org/10.1007/s12633-024-02996-9.

2. Katelyn J. Baumler, Raymond E. Schaak. Tutorial on describing, classifying and visualizing common crystal structures in nanoscale materials systems // ACS Nanoscience. – 2024. – Vol.4 (5). – P. 290-316. https://doi.org/10.1021/acsnanoscienceau.4c00010

3. Shin J. C., Chanda D., Chern W., Yu K. J., Rogers J. A., Li X. Experimental study of design parameters in silicon micropillar array solar cells produced by soft lithography and metal-assisted chemical etching // IEEE Journal of Photovoltaics – 2012. – Vol.2. – № 2. – P.129–133. https://doi:10.1109/JPHOTOV.2011.2180894

4. Botan Jawdat Abdullah., Size effect of band gap in semiconductor nanocrystals and nanostructures from density functional theory within HSE06 // Materials Science in Semiconductor Processing. – 2022. – Vol. 137. – P. 106214. https://doi.org/10.1016/j.mssp.2021.106214

5. Yao B., Shaopeng W., Jun H., Shuitao G. Size and temperature effects on bandgap analysis of a defective phononic crystal beam // Crystals. – 2024. – Vol.14(2). – P.163. https://doi.org/10.3390/cryst14020163

6. Saeed M., Ur Rehman S., Khan M. M., Uddin Z. Computation of characteristics of C IV transitions // East European Journal of Physics. – 2023. – Vol. 2. – P. 165-172. https://doi.org/10.26565/2312-4334-2023-2-16

7. Ayoub R., AL-Timimi M. H., Abdullah M. Enhancements of structural and optical properties of MgO: SnO2 nanostructure films // East European Journal of Physics. -2023. -Vol. 3. – P. 546-554. https://doi.org/10.26565/2312-4334-2023-3-64.

8. Borblik V.L. Analytic theory for current-voltage characteristic of a nanowire radial p-i-n diode // Semiconductor Physics, Quantum Electronics Optoelectronics. – 2021. – Vol.24(4). – P. 419-424. https://doi.org/10.15407/spqeo24.04.419

9. Ibeh G., Lawani C., Emmanuel J., Oyedare P., Danladi E., Ige O. Enhanced performance of CuIn1-xGxSe2 solar cell through optimization of absorber and buffer layer properties using SCAPS-1D // East European Journal of Physics. – 2021. – Vol.(3). – P.67-76. https://doi.org/10.26565/2312-4334-2022-3-09

10. Parida M. K., Sundari S. T., Sathiamoorthy V., Sivakumar S. Current-voltage characteristics of silicon PIN diodes irradiated in KAMINI nuclear reactor // Nuclear Instruments and Methods in Physics Research Section A: Accelerators, Spectrometers, Detectors and Associated Equipment. – 2018. – Vol. 905. – P. 129-137. https://doi.org/10.1016/j.nima.2018.07.014

11.Kolesnikova I., Lozinskaya A., Mihaylov T., Novikov V., Shemeryankina A., Sherbakov I., Zarubin A. Temperature dependencies of current-voltage characteristics of GaAs:Cr // Journal of Instrumentation. – 2016. – Vol. 11(3). – P. 03059–03059. https://doi.org/10.1088/1748-0221/11/03/C03059

12.Kurucova N., Šagátová A., Pavlovič M., Zaťko B., Kováčová E., Boháček P., Predanocy M. Experimental analysis of the electric field distribution in semi-insulating GaAs detectors via alpha particles // Journal of Instrumentation. – 2024. – Vol.19(3). – P.03049. https://doi.org/10.1088/1748-0221/19/03/C03049

13.Fahad O. A., Al-Rawi B. K., Ramizy A. Performance evaluation of multi layered ZnO/Ge/Si photodetector: the effect of pulses laser. Optical and Quantum Electronics. – 2024. – Vol. 56(8). – P. 1392. https://doi.org/10.1007/s11082-024-07309-3.

14.Borblik V.L., Electrostatics of the nanowire radial p-i-n diode // Semiconductor Physics, Quantum Electronics & Optoelectronics – 2019. Vol.22 (2). – P. 201-205. https://doi.org/10.15407/spqeo22.02.201

15.Su Q., Lin H., Wang G., Tang H., Xue C., Li Z., Gao P. Theoretical limiting□efficiency assessment on advanced crystalline silicon solar cells with Auger ideality factor and wafer thickness modifications. Progress in Photovoltaics: Research and Applications – 2024.- Vol. 32. № 9. P. 587-598. https://doi.org/10.1002/pip.3790

16. Liu Y., Zhang K., Feng F., Chan K. W., Yeung S. Y., Kwok H. S., Liu Z. The size and temperature effect of ideality factor in GaN/InGaN multiple quantum wells micro□light□emitting diodes // Journal of the Society for Information Display-2021.Vol. 29(12). – P. 948-960. https://doi.org/10.1002/jsid.1070

17. Borblik V.L., Concerning the depletion width of a radial p-n junction and its influence on electrical properties of the diode // Semiconductor Physics, Quantum Electronics & Optoelectronics. – 2017. – Vol. 20(2). – P. 168-172. https://doi.org/10.15407/spqeo20.02.168

18.Abdullayev J. Sh., Sapaev I. B. Optimization of the influence of temperature on the electrical distribution of structures with radial p-n junction structures // East Eur. J. Phys. – 2024. – Vol. 3. – P. 344 https://doi.org/10.26565/2312-4334-2024-3-39

19.Wong H. Y. Calibrated Si mobility and incomplete ionization models with field dependent ionization energy for cryogenic simulations // International Conference on Simulation of Semiconductor Processes and Devices (SISPAD) Kobe, Japan. – 2020. – P. 193-196. https://doi.org/10.23919/SISPAD49475.2020.9241599

20.Abdullayev J. Sh., Sapaev I. B. Optimizing the influence of doping and temperature on the electrophysical features of p-n and p-i-n junction structures // Eurasian Physical Technical Journal – 2024. – Vol. 21. – № 3(49). – P. 21–28. https://doi.org/10.31489/2024No3/21-28

21.Habibe B., Sertap A. Exact analytical solution of the diode ideality factor of a p-n junction device using Lambert W-function model // Turkish Journal of Physics. – 2007. – Vol. 31(1). – P.7-10. https://journals.tubitak.gov.tr/physics/vol31/iss1/2

22. Gyubong K. Multiscale calculation of carrier mobility in organic solids through the fine-tuned kinetic Monte Carlo simulation // Computational Materials Science. – 2023. – Vol. 218. – P. 111957 https://10.1016/j.commatsci.2022.111957

23.Tobehn-Steinhäuser I., Reiche M., Schmelz M., Stolz R., Fröhlich T., Ortlepp T. Carrier mobility in semiconductors at very low-temperatures // Engineering Proceedings. – 2021. – Vol. 6(1). – P. 86. https://doi.org/10.3390/I3S2021Dresden-10086

24.Pathak P., Deb D., Nath D. et al. Incomplete ionization-dependent carrier mobility in silicon-on-insulator n-p-n double-gate tunnel field-effect transistors // J. Electron. Mater. – 2024. – Vol.53. – P. 1142–1160. https://doi.org/10.1007/s11664-023-10852-6

25.Ma J., Nissimagoudar A. S., Li W. First-principles study of electron and hole mobilities of Si and GaAs // Physical Review B. – 2018. – Vol.97(4). – P.045201. https://doi.org/10.1103/PhysRevB.97.045201

26.Ramya M., Nagarajan K.K. Investigation of single event transients on RingFET using 3D TCAD simulations // Silicon – 2023. – Vol. 15. – P. 875–886. https://doi.org/10.1007/s12633-022-02055-1

27. Cai X.-Y., Yang J.-H., Wei Y. Suppression of the drift field in the p-type quasineutral region of a semiconductor p-n junction // Chinese Physics Letters. – 2012. Vol. 29(9). – P. 097202. https://doi.org/10.1088/0256-307X/29/9/097202

Information about authors:

Abdullayev Jo'shqin Shakirovich, Senior teacher at the Tashkent Institute of Irrigation and Agricultural Mechanization Engineers, National Research University. e mail: j.sh.abdullayev6@gmail.com

Sapaev Ibrokhim Bayramdurdievich, PhD, associate professor at the Tashkent Institute of Irrigation and Agricultural Mechanization Engineers, National Research University. e mail: sapaevibrokhim@.gmail.com